Journal of Solid State Chemistry **147,** 58–67 (1999)
Article ID jssc.1999.8158, available online at http://www.idealibrary.com on IDEAL®

Evidence of a Mixed-Valence State for Europium in the Misfit Layer Compound $[(EuS)_{1.5}]_{1.15}NbS_2$ by Means of a Superspace Structural Determination, Mössbauer Spectroscopy, and Magnetic Measurements

L. Cario, A. Lafond, P. Palvadeau, C. Deudon, and A. Meerschaut[1]

Institut des Matériaux de Nantes, UMR 6502 CNRS, Université de Nantes, Laboratoire de chimie des solides, 2 rue de la Houssinière, BP 32229, 44322 Nantes Cedex 03, France

Received October 22, 1998; in revised form December 24, 1998; accepted December 1998

DEDICATED TO THE MEMORY OF PROFESSOR JEAN ROUXEL

The complete structure of the misfit layer compound $[(EuS)_{1.5}]_{1.15}NbS_2$ is described as a (3+1)-dimensional intergrowth compound with two modulated subsystems ($v = 1$, 2, for NbS_2 and EuS, respectively) which have the (a^*_{v2}, a^*_{v3}) reciprocal-lattice plane in common. A superspace embedding follows from four reciprocal-lattice vectors given by $a_1^* = a_{11}^*$, $a_2^* = a_{12}^*$, $a_3^* = a_{23}^*$, and $a_4^* = a_{21}^*$. The symmetry is given by the superspace group $G_s = Fm2m$ ($\alpha 00$) with modulation wave vector $q = a_{21}^* = \alpha a_{11}^*$ ($\alpha = 0.5768(1)$). The structure of this composite compound is built up of an alternated sequence of two different types of slabs (i.e., NbS_2 (*H*-part) and EuS (*Q*-part)), stacked along the c direction. The *Q*-part is a three-atom-thick layer (Eu2S2-Eu1S1-Eu2S2). The NbS_2 subsystem has cell parameters $a_{11} = 3.3241(4)$ Å, $a_{12} = 5.7841(5)$ Å, and $a_{13} = 14.816(2)$ Å, with space group $Cm2m$. The EuS subsystem has lattice parameters $a_{21} = 5.7628(5)$ Å, $a_{22} = 5.7841(5)$ Å, and $a_{23} = 29.632(4)$ Å, with space group $Fm2m$. Refinements on 1721 unique reflections converged to $R = 3.58\%$ ($R_w = 4.75\%$) on a modulated structure model with 50 parameters. The largest modulation amplitudes occur on the outer Eu2 atoms. A bond-valence calculation using results from this structure determination shows that Eu atoms on the exterior sides (Eu2) of the EuS slab are in the +II oxidation state while inner Eu atoms (Eu1) are at the +III state. Mössbauer and magnetic measurements confirm the mixed-valence (Eu^{2+}/Eu^{3+}) state of this compound. A ferromagnetic long-range order appears below 7 K.

INTRODUCTION

The composite structure of the misfit layered chalcogenides $(MX)_{1+x}TX_2$ (where M = Sn, Pb, rare earth metals; T = Ti, V, Cr, Nb, Ta; X = S, Se; $1.08 < 1 + x < 1.28$) results from the alternate stacking of MX slabs (NaCl-type structure) and TX_2 slabs (edge-sharing octahedra for T = Ti, V, Cr or edge-sharing trigonal prisms for T = Nb, Ta). The incommensurate character is due to the fact that the ratio of the a parameters of the two sublattices is not a rational number.

Structural determination for these compounds can be made through the composite approach which consists of the structure determination of each part separately, and then in using common reflections ($0kl$) to fix the relative arrangement between both parts. In that procedure, modulation is not taken into account and satellite reflections are ignored. Each subsystem has its own 3 D space group and unit cell parameters. However, the true composite crystal structure lacks 3 D periodicity. Interaction between the two subsystems leads to a mutual modulation with a wavevector for one subsystem being dictated by the other subsystem. Then, the complete structure solution for the so-called incommensurate intergrowth compounds can only be provided by the superspace approach (1–5). In this approach, the modulation is taken into account which means that the interatomic distances between atoms within the same subsystem or belonging to different subsystems can be calculated. It is of great interest to know the amplitude of these modulated distances to determine which consequences are expected on the physical properties. For example, considering the case of $(LaS)_{1.19}CrS_2$, examination of the range of Cr–Cr distances within the modulated CrS_2 slab was of major interest in determining which type of magnetic interaction could occur (6). Another example is provided with some misfit layer phases where semiconducting behavior was explained by a carrier localization resulting from a nonperiodic potential generated from the modulated TX_2 structure (7, 8).

[1] To whom correspondence should be addressed.

0022-4596/99 $30.00

Recently, the structure of the title compound has been determined via the composite approach (9). In this paper, a study of the complete modulated structure of $[(EuS)_{1.5}]_{1.15}NbS_2$ is given, taking into account measurement of satellite reflections. Then, following this structural determination, Mössbauer, and magnetic studies were engaged.

STRUCTURE DETERMINATION

X-Ray Data Collection and Reduction

Synthesis conditions have been reported in a previous paper (9). Single crystal X-ray diffraction was performed at first on an Enraf–Nonius CAD4 diffractometer, and then on a STOE IPDS diffractometer, using Mo$K\alpha$ radiation ($\lambda = 0.71069$ Å). The CAD4 diffractometer was used to record main Bragg reflections for the two subsystems (NbS_2 and EuS) independently, but also for the first order satellite reflections via a selected file with predefined *hkl* indices, *h* being a noninteger (program Createhkl (10)). Another X-ray record with the same single crystal was done on the stoe IPDS device, with a long exposure time to get very weak reflections (generally satellite reflections); however, the θ-range ($\sin\theta/\lambda < 0.655$ Å^{-1}) is more restricted than for the CAD4 ($\sin\theta/\lambda = 0.8$ Å^{-1}). The QVECTORS program (11) was used to index reflections, plate by plate, in a (3 + 1)-dimensional space. Only satellite reflections up to the second order were measured to prevent too large an overlap between simulated spots. Thus, two subsets, one from the IPDS (main reflections and satellite reflections (1st and 2nd order)) the other from the CAD4 (main reflections and 1st satellite reflections) were available. Unit cell parameters refinement with the U-fit program (12) from 50 selected reflections collected on the CAD4 diffractometer and indexed in the (3 + 1)-dimensional space led to values $a_s =$ 3.3241 (4) Å, $b_s = 5.7841(5)$ Å, $c_s = 29.632(4)$ Å, $\alpha = a_{11}/a_{21} =$ 0.57682(13), and $V_s = 569.7(2)$ Å^3, for an orthorhombic symmetry. Table 1 summarizes all the details for both data collections.

The intensities were corrected for Lorentz and polarization effects, and for absorption (analytic method using a Gaussian integration); then, the two subsets of reflections were scaled. Data reduction, absorption corrections, Fourier calculations, and refinements were done with the JANA98 chain program (13).

An integer indexing of the complete diffraction pattern is obtained with four reciprocal vectors, $M^* = \{\mathbf{a}_1^*, \mathbf{a}_2^*, \mathbf{a}_3^*, \mathbf{a}_4^*\}$, chosen as: $\mathbf{a}_1^* = \mathbf{a}_{11}^*$, $\mathbf{a}_2^* = \mathbf{a}_{12}^*$, $\mathbf{a}_3^* = \frac{1}{2}\mathbf{a}_{13}^* = \mathbf{a}_{23}^*$, and $\mathbf{a}_4^* = \mathbf{a}_{21}^*$. The $\mathbf{a}_{vi}^*$ ($v = 1, 2$; $i = 1, 2, 3$) are the reciprocal-lattice vectors of the subsystem unit cell, with $v = 1$ for NbS_2 and $v = 2$ for EuS. Superspace is obtained in the usual way, by identification of the four basis vectors of M^* with the perpendicular projection of four independent translation vectors in a (3 + 1)-dimensional space (1, 2). The fourth element of M^* can be expressed in the first three. This defines the incommensurability, expressed by the σ matrix: $\sigma = (\alpha,0,0)$. The relation between the set M^* and the subsystem reciprocal lattices, and the subsystem modulation wavevectors is given by the matrices W^v according to (14,15):

$$\begin{pmatrix} \mathbf{a}_{v1}^* \\ \mathbf{a}_{v2}^* \\ \mathbf{a}_{v3}^* \\ q_v \end{pmatrix} = W^v \begin{pmatrix} \mathbf{a}_1^* \\ \mathbf{a}_2^* \\ \mathbf{a}_3^* \\ \mathbf{a}_4^* \end{pmatrix}$$

where

$$\begin{pmatrix} 1 & 0 & 0 & 0 \\ 0 & 1 & 0 & 0 \\ 0 & 0 & 1 & 0 \\ 0 & 0 & 0 & 1 \end{pmatrix} \quad \text{and } W^2 = \begin{pmatrix} 0 & 0 & 0 & 1 \\ 0 & 1 & 0 & 0 \\ 0 & 0 & 1 & 0 \\ 1 & 0 & 0 & 0 \end{pmatrix}.$$

The W^v matrices can be interpreted as defining a coordinate transformation in superspace, between the superspace axes corresponding to M^* and the standard superspace for each subsystem. For example, W^v gives the relation between the subsystem indexing of reflections and the indexing on M^*:

$$(H, K, L, M) = (h_v, k_v, l_v, m_v)W^v,$$

where (H, K, L, M) are the indices with respect to M^* and (h_v, k_v, l_v, mv) are the reflection indices with respect to M_v^* ($M_v^* = \{\mathbf{a}_{v1}^*, \mathbf{a}_{v2}^*, \mathbf{a}_{v3}^*, q^v\}$, $v = 1, 2$). Because W^1 is chosen to be the unit matrix, the h_1, k_1, l_1, m_1 and (H, K, L, M) indices are identical (16). From the CAD4 diffractometer, the 3 subsets of reflections (i.e., main reflections of NbS_2 and EuS, plus satellite reflections) with three indices were transformed to the superspace indexing (four-integer indices). Thus, $(H, K, L, 0)$ and $(0, K, L, M)$ indices correspond to main reflections of NbS_2 and EuS parts, respectively; (H, K, L, M) indices $(H, M \neq 0)$ correspond to satellite reflections. Systematic absences were found as $H + K + L = 2n + 1$, $H + K + M = 2n + 1$, and $L + M = 2n + 1$ for the (H, K, L, M) reflections; after their reject, 12035 are kept. Among the rejected reflections, very few satisfied the criterion $I > 3\sigma(I)$; these ones were of type $(4, K, L, M)$. Considering the incommensurate nature, the special value of $\alpha = 0.5768(1) \approx 4/7 = 0.57142$ determines a partial overlap between the $(4, K, L, M)$ reflections and the $(H, K, L, 7)$ reflections; this explains the presence of some reflections which violate the above extinction rules. The superspace group explaining all these extinctions is $G_s = Fm2m(\alpha,0,0)$. The 12,035 observed reflections averaged in agreement with the point group $(m2m, -1-11)$, gave a reliability factor $R_{int} = 4.3\%$ for reflections with $I > 3\sigma(I)$, that corresponds to 1721 of them among the 3990 independent ones.

TABLE 1
Crystallographic Data, Experimental Details, and Refinement Results for $[(EuS)_{1.5}]_{1.15}NbS_2$

Crystallographic data	NbS_2	EuS	Option (3 + 1)D
Structural formula	$Eu_{1.7304}NbS_{3.7304}$	$EuNb_{0.5768}S_{2.1536}$	$[(EuS)_{1.5}]_{1.1536}NbS_2$
Color		black	
Molar weight (g mol^{-1})	475.38	274.59	475.38
Crystal system		Orthorhombic	
Space group	*Cm*2*m*	*Fm*2*m*	*Fm*2*m* (α00)
Temperature (K)		293	
Cell parameters		25 reflections	50 reflections
a (Å)	3.3243(3)	5.762(1)	3.3241(4)
b (Å)	5.7844(8)	5.7837(5)	5.7841(5)
c (Å)	29.622(6)	29.637(7)	29.632(4)
			q = 0.57682(13)**a***
V (Å^3)	569.6(2)	987.7(3)	569.7(2)
Z	4	12	4
Calc density (g cm^{-3})	5.542	5.538	5.541
Crystal shape		platelet	
Crystal size (mm^3)		$\sim 0.260 \times 0.210 \times 0.008$	
Data collection	Enraf–Nonius CAD-4F	Stoe IPDS	
Monochromator	oriented graphite (002)		
Radiation	MoK-$L_{2,3}$ ($\lambda = 0.71069$Å)		
Scan mode	$\omega/2\theta$	ω	
Total recorded reflections	5935	6100	
hkl range	$-5 < h < 5$; $-7 < k < 7$	$-5 < h < 5$; $-9 < k < 9$	
	$-38 < l < 38$; $-2 < m < 2$	$0 < l < 46$; $-9 < m < 9$	
$\sin(\theta)/\lambda$ range	0–0.800	0–0.655	
Data reduction	Option (3 + 1)D		
Absorption coefficient (cm^{-1})	220.1		
Absorption correction	Analytic		
T_{min}/T_{max}	0.08/0.84	0.08/0.84	
Scaling factor CAD4/IPDS	0.4896(10) calculated from 781 common reflections $I > 10\sigma(I)$		
Total recorded reflections	12,035		
Independent reflections (R_{int}(obs))	3390 (0.043)		
Observed reflections ($I > 3\sigma(I)$)	1721		
Refinement results			
Refinement based on *F*	($F(000) = 839$)		
R/R_w (%)	3.58/4.75		
S	2.14		
No. of refinement parameters	50		
Weighting scheme	$w = 1/(\sigma^2\|F_o\| + (0.015)\|F_o\|)^2)$		
Residual electronic density e$^-$/Å^3	$[-3.3, +2.1]$		

*$R = \sum ||F_o| - |F_c|| / \sum |F_o|$. $R_w = [\sum w(|F_o| - |F_c|)^2 / \sum w|F_o|^2]^{1/2}$.

Structure Refinement

The structure of $[(EuS)_{1.5}]_{1.15}NbS_2$ was initially solved in the composite approach by considering, separately, reflections from EuS (space group *Fm*2*m*) and NbS_2 (space group *Cm*2*m*). The refined atomic positions have then been used to determine the complete average structure with the superspace group *Fm*2*m* (α,0,0). Refinement, conducted from the whole main reflections, converged at $R = 4.1\%$ for 30 variables and 6 atomic positions. The next step consisted of introducing the modulation functions for all atoms. Coordinates for any atom μ belonging to the subsystem ν, referred to the superspace, are dependent on the section *t*, i.e., of the phase. These coordinates can be expressed in the

subsystem M_v to which an atom belongs, with the following relations (3).

$$x^{\mu}_{vi} = \bar{x}^{\mu}_{vi} + u^{\mu}_{vi}(\bar{x}_{vs4}) \quad (v = 1, 2 \text{ and } i = 1, 2, 3),$$

where $\bar{x}^{\mu}_{vi}$ is the basic-structure coordinates:

$\bar{x}^{\mu}_{1i} = n_{1i} + x^{0}_{1i}(\mu)$ $(i = 1, 2, 3)$ for the first subsystem (NbS_2),

$\bar{x}^{\mu}_{21} = n_{21} + x^{0}_{21}(\mu) - t$ and $\bar{x}^{\mu}_{2i} = n_{2i} + x^{0}_{2i}(\mu)$ $(i = 2, 3)$ for the second subsystem (EuS)

n_{vi} is a translation of sublattice v and $x^{0}_{vi}(\mu)$ is the basic-structure position of the μ atom relative to the unit cell.

Modulation functions (periodicity of 1 with respect to $\bar{x}_{vs4}$) can be developped in Fourier series:

$$u^{\mu}_{vi}(\bar{x}_{vs4}) = \sum_{n=1}^{\infty} [A^{\mu}_{ni} \sin(2\pi n \bar{x}_{vs4}) + B^{\mu}_{ni} \cos(2\pi n \bar{x}_{vs4})].$$

Observation of the difference-Fourier map was essential to introduce the modulation functions. High residual peaks ($\pm 5\ e^{-}/Å^3$) were observed all around Eu1 and Eu2 atoms; their distribution, in the superspace, is characteristic of a modulation effect (see Fig. 1a). Account of a displacive modulation function for both Eu atoms has improved the reliability factor ($R = 4.0\%$ for all reflections and $R = 3.5\%$ for the main ones) and reduced the height of residuals (see Fig. 1b). If one applies modulation on all atoms, refinement with 49 variables converged at $R = 3.67\%$ for all reflections (mains + satellites = 1721) and at $R = 3.34\%$ for the main reflections. Applying the test for a twinning that relates the two enantiomorphs led to a ratio of 35(3)% and a small lowering of the R value ($R = 3.58\%$ for all reflections with 50 variables). Table 2 summarizes the fractional coordinates (IIa), the anisotropic thermal factors (IIb), and the modulation parameters (IIc).

Structure Description

Figures 2a,b show the projection of the structure of $[(EuS)_{1.5}]_{1.15}NbS_2$ onto the (b,c) plane and (a,c) plane, respectively. [EuS] and [NbS_2] slabs regularly alternate along the stacking c-direction. [EuS] slabs are a three-EuS-layer-thick instead of two as examplified by most of the misfit layer compounds $(MX)_{1+x}TX_2$ (17). Two crystallographically independent positions are found for Eu atoms: Eu2 atoms located on the exterior sides and Eu1 atoms situated in the middle of the [EuS] slab. Eu2 atoms, which protrude the S2 planes, are coordinated by five S atoms belonging to the [EuS] part, and by 1 or 2 S atoms from the [NbS_2] part. Eu1 atoms are coordinated by six S atoms (4S1 and 2S2) distributed over a distorted octahedral arrangement. The [NbS_2] part is quasi identical to the one observed in the binary NbS_2 compound, i.e., Nb atoms in

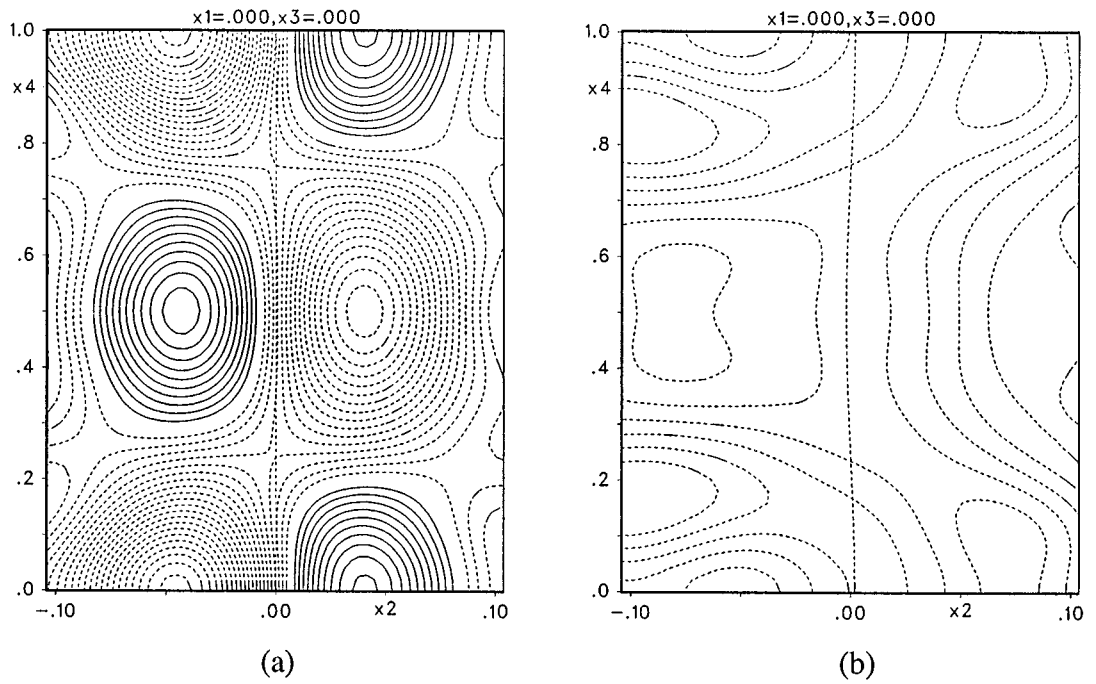

FIG. 1. Difference-Fourier maps around Eu1 (a) without taking into account the modulated feature of the structure and (b) taking into account the modulated feature of the structure (each line corresponds to $0.25\ e^{-}/Å^3$).

TABLE 2
Fractional Atomic Coordinates (a), Atomic Displacement (b), and Displacive Modulation Coefficients (c) for $[(EuS)_{1.5}]_{1.15}NbS_2$

(a) Atom	v	Mult.	Occ.	X	Y	Z	U_{eq}
Nb	1	4	1	0	−0.0798(3)	1/4	0.0085(1)
S	1	8	1	0	0.2530(3)	0.19737(3)	0.0103(3)
Eu1	2	4	1	0	0	0	0.0121(1)
Eu2	2	8	1	0	0.4980(3)	0.11209(1)	0.01385(8)
S1	2	4	1	0	0.495(1)	0	0.0139(6)
S2	2	8	1	0	−0.0009(7)	0.09041(5)	0.0132(3)

(b) Atom	U_{11}	U_{22}	U_{33}	U_{12}	U_{13}	U_{23}
Nb	0.0131(2)	0.0052(1)	0.0072(2)	0	0	0
S	0.0160(5)	0.0073(3)	0.0075(6)	0	0	−0.0005(3)
Eu1	0.0160(2)	0.0097(1)	0.0106(2)	0	0	0
Eu2	0.0171(1)	0.0095(1)	0.0149(1)	0	0	−0.0003(2)
S1	0.016(1)	0.0096(7)	0.0164(9)	0	0	0
S2	0.0181(7)	0.0099(5)	0.0116(5)	0	0	−0.002(1)

(c) Atom (μ)	v	n	A^{μ}_{n1}	B^{μ}_{n2}	B^{μ}_{n3}
Nb	1	1	0	0	0.00023(4)
		2	−0.0070(6)	−0.0004(2)	0
S	1	1	−0.003(3)	−0.0020(2)	−0.0023(2)
Eu1	2	1	0.0043(5)	0.00162(10)	0
Eu2	2	1	0.0022(3)	0.01135(6)	−0.00058(4)
		2	−0.0008(2)	0.0001(2)	0.00075(5)
S1	2	1	0.014(2)	0.0019(5)	0
S2	2	1	−0.0010(15)	0.0061(3)	−0.0003(2)

a trigonal prismatic coordination of S atoms. The main difference with results deduced from the composite approach consists of the calculated interatomic distances which, now, depend on the section t. Table 3 summarizes the main interatomic distances and makes a comparison between calculated distances from the basic structure and the range of distances (minima, maxima, and averages) from the modulated structure model. The most modulated interatomic distances are between atoms Eu2 (subsystem 2) and S (subsystem 1) which are located at the interface between the two subsystems (see Fig. 3).

The bond valence method (13,18,19) was used to calculate the valence of the two crystallographically different Eu atoms, according to equations:

$$v_{ij} = \exp[(R^{\circ}_{ij} - d_{ij})/b] \quad \text{and} \quad V_i = \sum v_{ij},$$

where $b = 0.37$ is a universal constant and R°_{ij} depends on the chemical nature of both elements; the interatomic distance between i and j atoms is d_{ij}. For periodic crystals, the summation is over all the j atoms of the coordination sphere. The valence is a function of the interatomic distance, and thus becomes a periodic function of t in incommensurate crystals (3). Figure 4 shows the variation of calculated valences for Eu1 and Eu2 atoms as a function of t. It clearly indicates that Eu1 atoms (in the middle plane of EuS) and Eu2 atoms (protruding the EuS slab) have an oxidation state in the range 2.8-3.0 and 1.8-2.0, respectively.

PHYSICAL PROPERTIES

Mössbauer Spectroscopy

Mössbauer spectra were obtained with a constant acceleration automatic folding Elscint type spectrometer using a room temperature $^{131}SmF_3$ source in a transmission geometry. The Mössbauer sample was studied in the 4–300 K temperature range with an Oxford Instruments variable-temperature cryostat. The spectra were computed with a least-squares routine using Lorentzian lines. The isomer shift values of this europium niobium sulfide were calculated in relation with the resonance line of Eu_2O_3.

Figure 5 shows the Mössbauer spectra recorded at various temperatures. Between 300 and 8 K spectra were characterized by the presence of two singlets. The values of the isomer shifts obtained at 300 K were $\delta = -0.19$ and -12.3 mm s^{-1}. Main values are gathered in Table 4. The two well-resolved lines with nearly 40/60 intensity ratio can be attributed to Eu^{3+} and Eu^{2+}, respectively. Isomer shift values are in good agreement with values reported in the literature for europium sulfides. The singlet corresponding to Eu^{2+} is asymmetric and it is well fitted with the superposition of two singlets, in relation with the site modulation. However at low temperature, this modulation vanishes and on the spectra recorded at 8 K, the line corresponding to Eu^{2+} is perfectly symmetric. Between 300 and 8 K the isomer values, within the experimental accuracy, can be considered as constant.

The situation is very different from Eu_3S_4 in which europium atoms occupy only one crystallographic site. At room temperature, the charge fluctuation frequency is fast compared to the Mössbauer frequency and only a single line corresponding to $Eu^{2.67+}$ is observed, the splitting Eu^{2+}–Eu^{3+} occurring at low temperature (20,21) Eu_3S_4 is known to be a good example of an inhomogeneous mixed-valence state (22).

At 6.2 K and below, the Mössbauer spectra consist of an hyperfine Zeeman pattern corresponding to the magnetic ordering of Eu^{2+}, and a single line to Eu^{3+}, even if this line is partially overlapped by the Zeeman contribution. The ordering temperature is very low and for this reason, we have not followed the hyperfine field evolution. The transition temperature determined from magnetic measurements is 7 K (see below), in perfect agreement with Mössbauer spectra. Moreover, the magnetic moment at saturation also results only in the ordering of the Eu^{2+} sublattice.

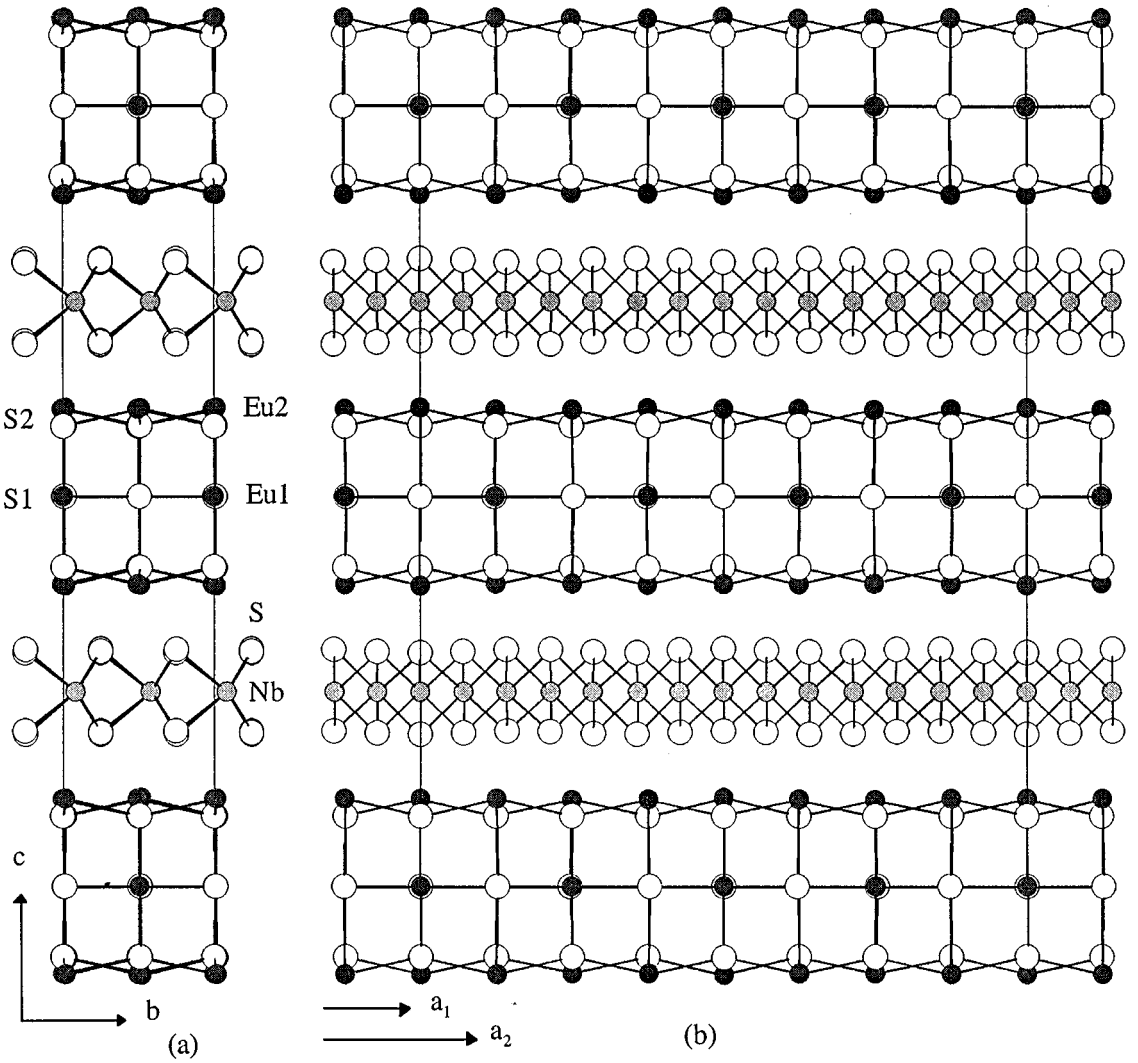

FIG. 2. Projection of the structure of $[(EuS)_{1.5}]_{1.15}NbS_2$ (a) onto the (b, c) plane and (b) onto the (a, c) plane. This drawing was done for the commensurate approximation of 4/7.

Magnetic Susceptibility Measurements

The temperature and field dependent data were recorded on a Quantum Design MPMS SQUID magnetometer. The temperature range was 5–300 K on a magnetic strength up to 50 kOe. Temperature dependent magnetization was measured from a powder sample ($m = 77.20$ mg). Isothermal measurements at low temperature were made from a crystal-stacked sample ($m = 1.48$ mg). In the latter case, the magnetic field was applied in a direction parallel to the c axis. Raw data were corrected for the sample holder contribution and for the diamagnetic contribution of the core electrons (-2.26×10^{-4} emu mol^{-1})

The magnetic susceptibility data for $[(EuS)_{1.5}]_{1.15}NbS_2$ are illustrated as a χT versus T curve in Fig. 6. The deviation from a constant value clearly indicates a transition to a long range ferromagnetic order with a Curie temperature of about 7 K. This transition temperature is lower than that of the monosulfide EuS (16.5 K (23)). The quadratic sublattice of the misfit compound has the NaCl structure type arrangement as also exhibited by the binary compound EuS. Obviously, due to the composite feature in the misfit compound, the Eu–Eu magnetic interactions have a 2D-character unlike in the europium monosulfide.

Figure 7 shows the inverse magnetic susceptibility as a function of temperature. A Curie–Weiss fit ($\chi = C/(T - \theta)$) of the data in the 10–300 K range yields a Curie constant of 9.98(1) cm^3 K mol^{-1} for one formula unit (1.725 Eu). The positive value of the Weiss temperature ($\theta = +5.0(1)$ K) is consistent with the ferromagnetic character of the magnetic interactions. The Curie constant for one mole of europium atoms (5.79 cm^3 K mol^{-1}) is quite smaller than that

TABLE 3
Main Interatomic Distances (Å) in $[(EuS)_{1.5}]_{1.15}NbS_2$

Bond	Sym. operation	Basic structure	Modulated structure		
			Average	Minimum	Maximum
Nb–Nb (×2)	$-1+x, y, z$ $1+x, y, z$	3.3241	3.3239	3.3024	3.3458
–Nb (×4)	$-\frac{1}{2}+x, -\frac{1}{2}+y, z$ $-\frac{1}{2}+x, \frac{1}{2}+y, z$ $\frac{1}{2}+x, -\frac{1}{2}+y, z$ $\frac{1}{2}+x, \frac{1}{2}+y, z$	3.3356(21)	3.3358	3.3129	3.3588
–S (×2)	x, y, z $x, y, \frac{1}{2}-z$	2.4774(20)	2.4783	2.4415	2.5184
–S (×4)	$-\frac{1}{2}+x, -\frac{1}{2}+y, z$ $\frac{1}{2}+x, -\frac{1}{2}+y, z$ $-\frac{1}{2}+x, -\frac{1}{2}+y, \frac{1}{2}-z$ $\frac{1}{2}+x, -\frac{1}{2}+y, \frac{1}{2}-z$	2.4759(11)	2.4765	2.4312	2.5406
Eu1–S1	$x, -1+y, z$	2.9210(58)	2.9214	2.9195	2.9229
–S1	x, y, z	2.8631(58)	2.8632	2.8612	2.8646
–S1 (×2)	$-\frac{1}{2}+x, -\frac{1}{2}+y, z$ $\frac{1}{2}+x, -\frac{1}{2}+y, z$	2.8816(1)	2.8823	2.7842	2.9791
–S2 (×2)	x, y, z $x, y, -z$	2.6790(15)	2.6790	2.6707	2.6875
–Eu1 (×4)	$-\frac{1}{2}+x, -\frac{1}{2}+y, z$ $-\frac{1}{2}+x, \frac{1}{2}+y, z$ $\frac{1}{2}+x, -\frac{1}{2}+y, z$ $\frac{1}{2}+x, \frac{1}{2}+y, z$	4.0825	4.0828	4.0485	4.1168
Eu2–S1	x, y, z	3.3215(3)	3.3220	3.2983	3.3610
–S2	x, y, z	2.9563(43)	2.9570	2.9346	2.9897
–S2	$x, 1+y, z$	2.9688(43)	2.9683	2.9412	3.0043
–S2 (×2)	$-\frac{1}{2}+x, \frac{1}{2}+y, z$ $\frac{1}{2}+x, \frac{1}{2}+y, z$	2.9523(3)	2.9530	2.9376	2.9731
–S	$-, y, z$	2.8972		2.8731	
–S	$-, \frac{1}{2}+y, z$	2.9260		2.9901	
–Eu2 (×4)	$-\frac{1}{2}+x, -\frac{1}{2}+y, z$ $-\frac{1}{2}+x, \frac{1}{2}+y, z$ $\frac{1}{2}+x, -\frac{1}{2}+y, z$ $\frac{1}{2}+x, \frac{1}{2}+y, z$	4.0825(17)	4.0840	4.0018	4.1746

N.B. The standard deviations do not take into account errors on the cell parameters.

expected for Eu^{2+} (7.88 cm^3 K mol^{-1}). The structure determination showed that a mixed-valence state for europium is expected in $[(EuS)_{1.5}]_{1.15}NbS_2$. Eu^{3+} is known to be a Van Vleck ion (24) with a small temperature dependent susceptibility (25) compared to that of Eu^{2+}, leading to a temperature dependent value of the effective moment; $\mu_{eff} = 3.4\ \mu_B/Eu^{3+}$ at room temperature (26). The contribution of Eu^{3+} for the magnetic behavior of $[(EuS)_{1.5}]_{1.15}NbS_2$ is certainly rather small. Assuming that $\frac{2}{3}$ of the Eu atoms are Eu^{2+} one calculates a Curie constant of 9.06 cm^3 K mol^{-1} for one formula unit. The difference between this value and the experimental one corresponds to the Eu^{3+} contribution: $C(Eu^{3+}) = 1.6$ cm^3 K mol^{-1}. This value is very close to the one deduced from the room temperature value of the effective moment (1.4 cm^3 K mol^{-1} (Eu^{3+})).

The low-temperature (5 K) field dependent magnetization is given in Fig. 8. The magnetization of this compound is approaching saturation by 50 kOe with value of 5.92 μ_B/Eu^{2+} (assuming that only Eu^{2+} ions have a magnetic contribution at this low temperature). This experimental value is not far away from the theoretical value of 7 μ_B/Eu^{2+}. Comparing the first magnetization curve to the Brillouin function (see inset in Fig. 8), one can see that only a very small fraction of the sample gets a magnetization under a low applied field. This result means that the easy magnetization direction is not parallel to the *c* axis.

In an incommensurate compound, one can expect that magnetic interactions are affected by the modulated feature of the atomic distances. But, the 4*f* orbitals in lanthanide elements are deep and are screened by the 5*s* and 5*p* closed

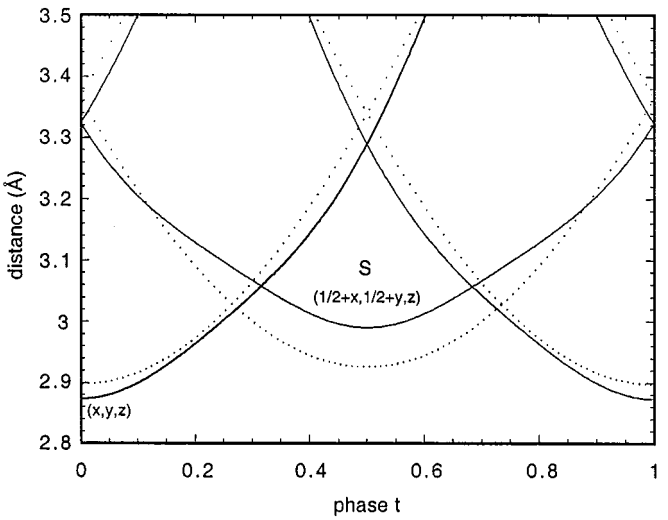

FIG. 3. Interactomic distances between Eu2 (subsystem 2) and S (subsystem 1) as a function of the phase t in the basic structure (dotted line) and in the modulated structure (solid line).

shells. Thus, magnetic interactions between $4f$ electrons are weakly sensitive to variation in Ln–Ln distances. This explains the low Curie temperature ($T_c = 7$ K) and the classic ferromagnetic behavior of $[(EuS)_{1.5}]_{1.15}NbS_2$.

DISCUSSION AND CONCLUDING REMARKS

Even though the modulated character of the structure is well ascertained looking at the distribution of interatomic distances (see Table 3), its "perturbating" effect does not seem apparent in the magnetic properties. Indeed, the observed ferromagnetic behavior is quite comparable with any standard ferromagnet; thus, for instance, the parent binary EuS compound which exhibits a nonmodulated NaCl structure type shows a similar ferromagnetic behavior. With regard to the Mössbauer spectroscopy, the incidence from the modulated structure is only seen on the peak enlargement. In any case, Mössbauer and magnetic measurements clearly indicate a mixed-valence state for europium. From bond valence calculations, taking into account the modulated character of the structure, this mixed-valence state (Eu(II) and Eu(III)) is also demonstrated.

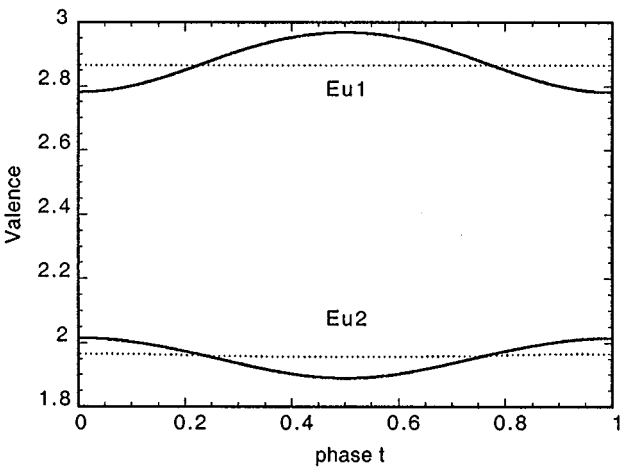

FIG. 4. Variation of the periodic function of the calculated valences versus the phase t for the two crystallographically different Eu1 and Eu2 atoms.

TABLE 4
Isomer Shifts (Eu_2O_3 as reference) and Linewidth Values Deduced from Mössbauer Spectra Recorded at Various Temperatures

T	δ (mm/s)	W (mm/s)*	%
	−0.19	1.19	40
300 K	−11.27	1.27	36
	−13.43	1.50	24
	−0.07	1.36	39
100 K	−11.03	1.03	18
	−12.91	2.03	43
	−0.13	1.37	38
77 K	−11.26	1.25	30
	−13.42	1.84	32
8 K	−0.13	1.47	37
	−12.17	2.19	63
	−27.92	1.72	4.5
	−21.17	1.48	11.5
	−15.62	2.20	22
6.2 K	−10.22	2.16	12.5
	−4.68	2.80	27
	−0.95	1.29	3.5
	3.92	2.25	12
	14.05	2.27	7
	−28.88	1.66	4
	−21.86	1.77	14
	−15.77	2.17	21
4.2 K	−9.07	2.28	17
	−3.74	2.48	20
	−0.32	1.33	6.5
	5.28	1.74	9.5
	16.50	2.11	8

*W, half-width at half-height.

The presence of Eu^{3+} needed for the stability of such a structure can be explained as follows. Band structure calculations have shown that rare-earth misfit compounds $(LnS)_{1+x}TS_2$ ($1Q/1H$) can be considered as intercalation compounds, the intercalated species being the LnS layers within the 2D TS_2 host matrix (27). Thus a strong electron transfer from the LnS part (donor: $Ln^{3+}e^-S^{2-}$, up to $1e^-$ to transfer) to the TS_2 part (acceptor) appears. The rigid band model can then be used to explain the band structures of these compounds: except the adjustment of the Fermi levels, the electronic structure is approximately a superposition

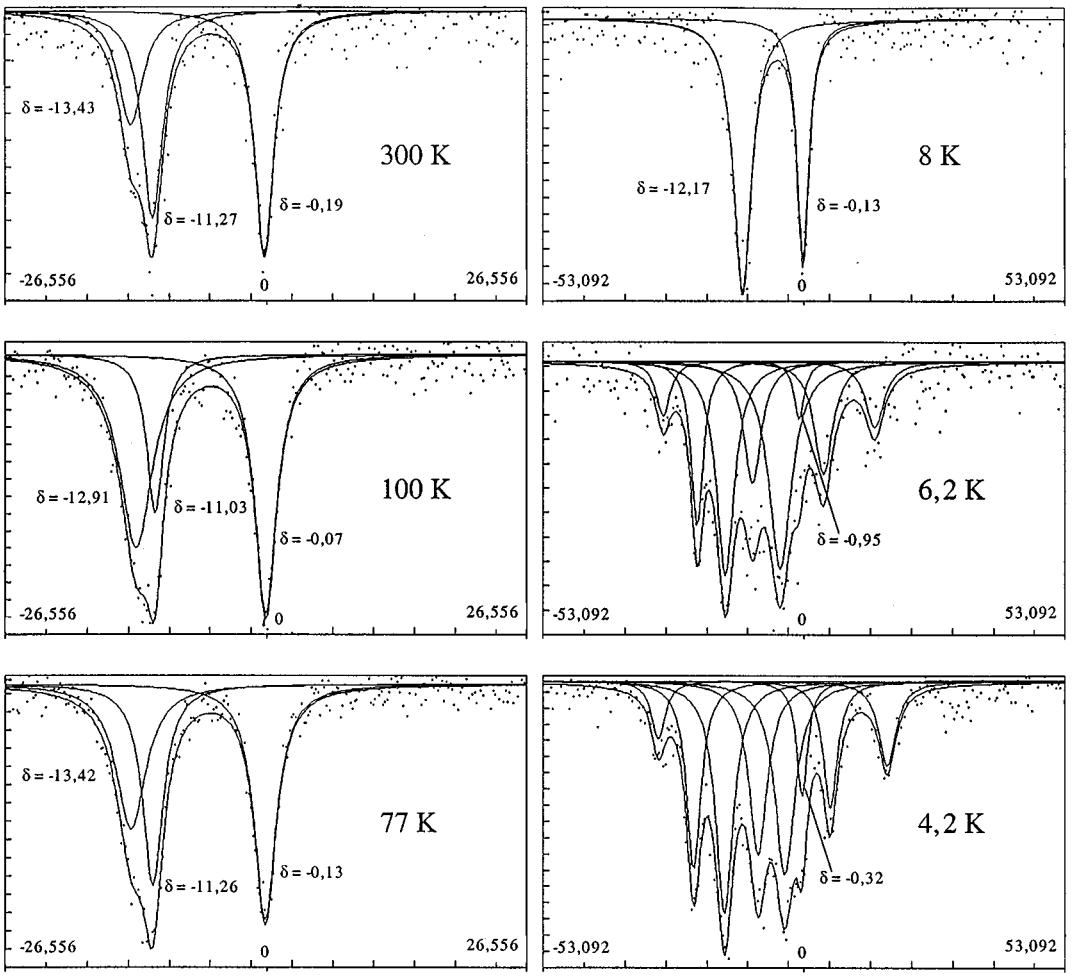

FIG. 5. Evolution of the Mössbauer spectra between 300 and 4.2 K. At low temperature, the splitting of the signal shows the magnetic ordering of Eu^{2+}.

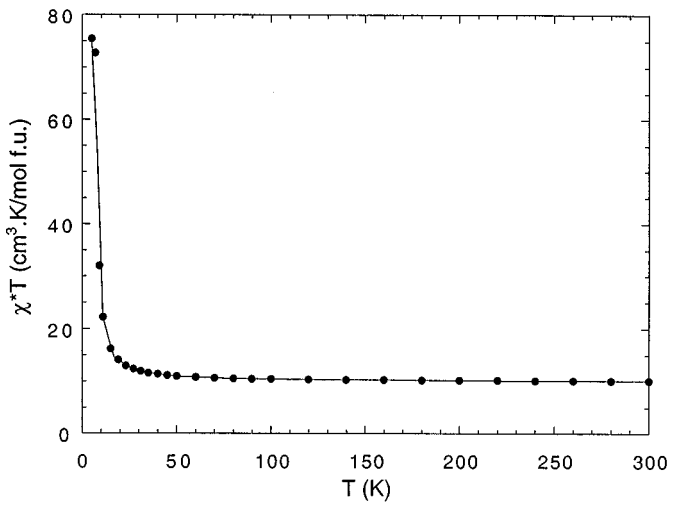

FIG. 6. Variation of (χT) as a function of temperature for $[(EuS)_{1.5}]_{1.15}NbS_2$. At low temperature, the dramatic increasing corresponds to the ferromagnetic transition.

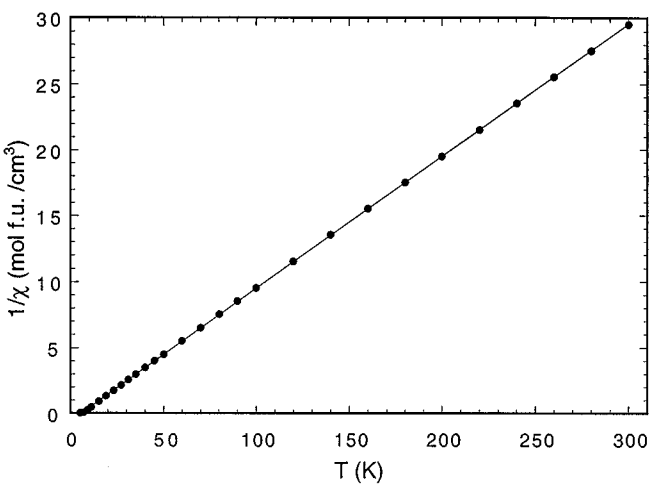

FIG. 7. Inverse magnetic susceptibility from 5 to 300 K. $[(EuS)_{1.5}]_{1.15}NbS_2$ obeys the Curie–Weiss law $[C/(T-\theta)]$ down to 10 K with $C = 9.98(1)\,cm^3\,K\,mol^{-1}$ for one formula unit and $\theta = +5.0(1)$ K.

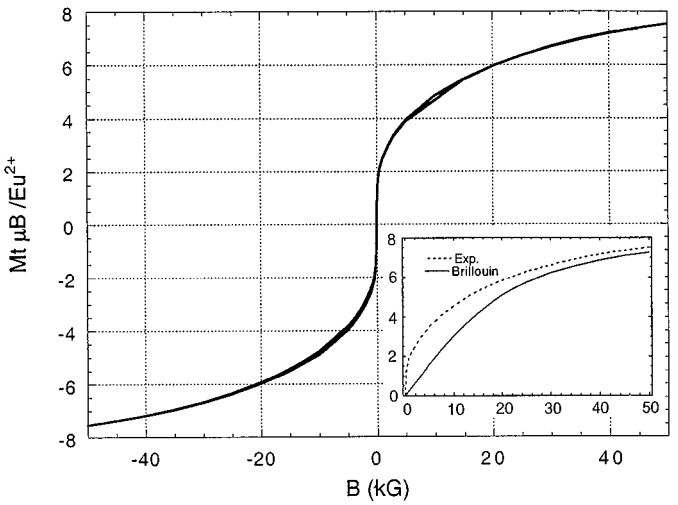

FIG. 8. Isothermal magnetization versus applied field. No hysteresis is observed. The inset compares the first magnetization curve with the Brillouin function.

of the electronic structures of each of the separate components, LnS and TS_2. Therefore, the stability of the misfit compounds is due to the strong charge transfer between layers; this transfer results from the high oxidation state (around $+3$) of the rare earth element. Such a high oxidation state is achieved for the misfit compound $(LaS)_{1.14}NbS_2$ and even for $(SmS)_{1.19}NbS_2$ which contain La^{3+} and Sm^{3+} ions, respectively (28). But from Sm to Eu, the decrease in energy of the 4*f* orbitals stabilizes the $+2$ oxidation state for Eu atoms. Thus, for a misfit compound $(EuS)_{1+x}NbS_2$ with only Eu^{2+} ions, there will be no transfer and the structure will not be stable. On the other hand, an EuS part with a mixed valence state for the Eu atoms could stabilize such a misfit structure type. This is the case for the misfit $[EuS)_{1.5}]_{1.15}NbS_2$ where the donor character of the EuS part is restored by the presence of Eu^{3+} in the center of the slab.

REFERENCES

1. A. Janner and T. Janssen, *Acta Crystallogr. A* **36,** 408 (1980).
2. P. M. de Wolff, T. Janssen, and A. Janner, *Acta Crystallogr. A* **37,** 625 (1981).
3. S. van Sammlen, *Crystallogr. Rev* **4,** 148 (1995).
4. S. van Smaalen, "Materials Science Forum" (A. Meerschaut, Ed.), Vols. 100 and 101, p. 205. Trans. Tech. Publications, Zürich, 1992.
5. V. Petricek, K. Maly, P. Coppens, X. Bu, I. Cisarova, and A. Frost-Jensen, *Acta Crystallogr. A* **47,** 210 (1991).
6. A. Lafond, A. Meerschaut, J. Rouxel, J. L. Tholence, and A. Sulpice, *Phys. Rev. B* **52**(2), 1112 (1995).
7. T. Kondo, K. Suzuki, and T. Enoki, *Solid State Commun.* **84**(10), 999 (1992).
8. L. Cario, J. Rouxel, O. Chauvet, Y. Moëlo, B. Corraze, and A. Meerschaut, *J. Phys.: Condens. Matter*, to be submitted (1998).
9. L. Cario, A. Meerschaut, C. Deudon, and J. Rouxel, *C.R. Acad. Sci. Paris* **1**(IIc), 269 (1998).
10. M. Evain, personal program, IMN—CNRS, Nantes, France.
11. "STOE-IPDS Software Manual, V2.75." STOE&Cie, Darmstadt, Germany, 1996.
12. M. Evain, "U-FIT: A cell parameter refinement program." IMN—CNRS, Nantes, France, 1992.
13. V. Petricek and M. Dusek, "JANA98: Crystallographic computing system." Institute of Physics, Academy of Sciences of the Czech Republic, Prague, 1998.
14. S. van Smaalen, *J. Phys. Condens. Matter* **1,** 2791 (1989).
15. S. van Smaalen, *Phys. Rev. B* **43,** 11330 (1991).
16. S. van Smaalen and J.L. de Boer, *Phys. Rev. B* **46(**5), 2750 (1992).
17. G. A. Wiegers and A. Meerschaut, "Materials Science Forum" (A. Meerschaut Ed.), Vols. 100 and 101, p. 101, Trans. Tech. Publications, Zürich, 1992.
18. I. D. Brown, *in* "Structure and Bondings in Crystals" (O'Keeffe and A. Navrotsky, Eds.), Vol. 2, p. 1. Academic Press, New York, 1981.
19. M. O'Keeffe, *Structure Bonding* **71,** 161 (1989).
20. E. Gorlich, H. U. Hrywkiewicz, K. Lakta, and K. Tomala, *in* "Proceedings of 5th International Conference on Mossbauer Spectroscopy," (J. Hucl and T. Zemak, Eds.), Vol. 3, pp. 557–560, 1975.
21. E. Gorlich, H. U. Hrywkiewicz, R. Kmiec, K. Lakta, and K. Tomala, *Phys. Stat. Solid.* **64,** 147 (1974).
22. O. Berkooz, *J. Phys. Chem Solids* **30**(1), 763 (1969).
23. P. Heller and G. Benedek, *Phys. Rev. Lett.* **10,** 71 (1965).
24. J. H. Van Vleck, "The Theory of Electric and Magnetic Susceptibilities," p. 232. Oxford Univ. Press, London, 1965.
25. (a) R. Saez Puche, M. Norton, T. R. White, and W. S. Glaunsinger, *J. Solid State Chem.* **50,** 281 (1983). (b) C. Cascales, R. Saez-Puche, and P. Porcher, *J. Solid State Chem.* **114,** 52 (1995).
26. C. Kittel, "Introduction of solid state physics." John Wiley and Sons Inc., New York, 1971.
27. C. M. Fang, S. van Smaalen, R. A. de Groot, C. Haas, and G. A. Wiegers, *J. Phys.: Condens. Matter* **8,** 5367 (1996).
28. O. Peña, P. Rabu, and A. Meerschaut, *J. Phys.: Condens. Matter* **3,** 9929 (1991).